Modal Analysis of a Deployable Truss Using the Finite Element Method

David V. Hutton*
Washington State University, Pullman, Washington

Development of a large-scale space station will require similarly large structural elements capable of assembly, fabrication, or deployment in space. Weight and volume constraints of the Space Shuttle Orbiter payload bay make deployable structures with minimum on-orbit assembly requirements the favored alternative. Current deployable structure concepts involve folding, three-dimensional trusses with automated deployment/retraction systems having high deployed-to-stowed volume ratios. Such designs employ a large number of pin joints to allow the rotational motion required for deployability. To assess the dynamic characteristics of a deployable space truss, a finite element model of the Science and Applications Space Platform truss has been formulated. The model incorporates all additional degrees of freedom associated with the pin-jointed members. Comparison of results with Structural Performance and Redesign models of the truss shows that the joints of the deployable truss affect the vibrational modes of the structure significantly only if the truss is relatively short.

Nomenclature

$\boldsymbol{A}$	= coordinate transformation matrix
$\boldsymbol{k}_e$	= element stiffness matrix in element frame
$\boldsymbol{k}$	= element stiffness matrix in global frame
$\boldsymbol{K}$	= system stiffness matrix
$\boldsymbol{L}_e$	= locator matrix for displacements
$\boldsymbol{m}_e$	= element consistent mass matrix in element frame
$\boldsymbol{m}$	= element consistent mass matrix in global frame
$\boldsymbol{M}$	= system consistent mass matrix
N	= total system degrees of freedom
T	= kinetic energy
$\boldsymbol{u}$	= vector of element displacements
$\boldsymbol{u}_g$	= element displacements in global frame
$\dot{\boldsymbol{u}}$	= vector of element velocities
$\boldsymbol{U}$	= vector of system displacements
$\dot{\boldsymbol{U}}$	= vector of system velocities
$\ddot{\boldsymbol{U}}$	= vector of system accelerations
V	= potential energy
X, Y, Z	= Cartesian coordinates

Introduction

WITH the Space Transportation System (the Space Shuttle) now operational, the next logical step in mankind's use of space is the development of a permanent manned space station.[1] Construction of such a large-scale structure on-orbit will require similarly large structural elements which can be delivered via the Shuttle Orbiter's payload bay. Research and development activities in this area have been ongoing for several years. From these studies have evolved two major structural element concepts: 1) on-orbit fabrication of continuous truss-type "beams," and 2) deployable truss configurations having automatic deployment/retraction systems and high deployed-to-retracted volume ratios. Deployable concepts are currently in favor because of the flexibility afforded in constructing various platform shapes and since, being self-contained, no additional payload in the form of fabrication machinery is required.

A Structural Assembly Demonstration Experiment (SADE) has been proposed for STS Flight 28 scheduled for 1985. Each of five configuration options for SADE involves deployment and/or assembly of a truss-type structure as a cantilever from the payload bay of the Orbiter. Among the objectives of SADE are: testing of truss deployment and retraction systems, validation of connector designs for joining structural sections, data collection on extra vehicular activity (EVA) assembly tasks, and experimental evaluation of dynamic models of the truss structures. Of the five SADE options, four incorporate a structural design known as the Science and Applications Space Platform (SASP) truss. The SASP truss is a deployable three-dimensional structure which is intended to be a building-block element in the construction of a large-scale platform. The basic unit of the truss is a folding cell composed of two bays as shown in Fig. 1. When fully deployed, each bay has the overall dimensions of a 1.4-m cube. Theoretically, any number of cells can be joined end-to-end to create a deployable truss of arbitrary length. Alternatively, several independent trusses can be joined to construct a composite platform in a variety of shapes.

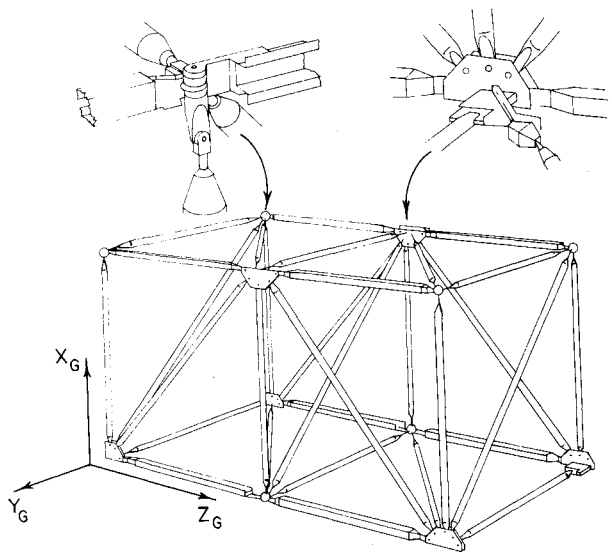

Fig. 1 Two-bay cell unit of the SASP-deployable truss.

A full-scale, ten-bay prototype of the SASP truss has been constructed for ground testing of deployment characteristics. A mathematical model of deployment dynamics also has been developed.[2] In addition to deployment testing and analysis, determination of the vibration modes of the fully deployed truss is required. For SADE, knowledge of truss dynamic

Received Jan. 4, 1983; revision received Sept. 5, 1983. Copyright © American Institute of Aeronautics and Astronautics, Inc., 1984. All rights reserved.

*Assistant Professor, Department of Mechanical Engineering.

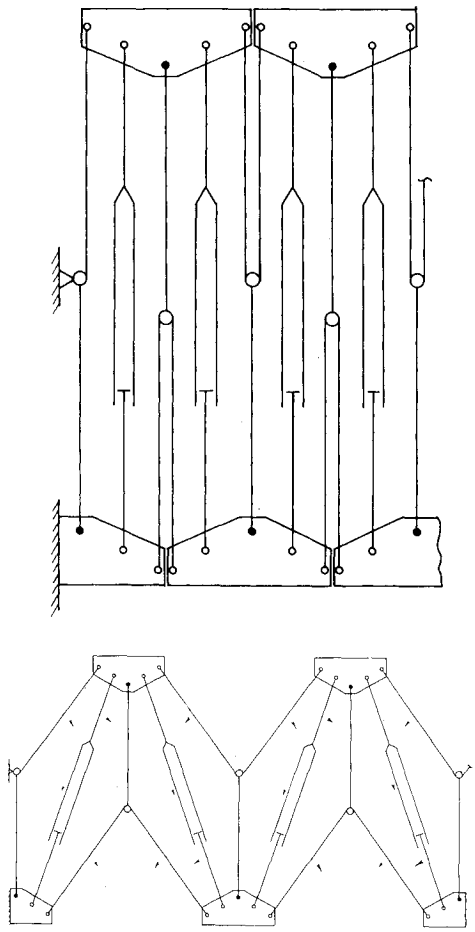

Fig. 2 Truss deployment details: a) retracted, b) deploying.

characteristics is a must since adverse low-frequency dynamic interaction could affect Orbiter control during the flight experiment. Longer range, dynamic analysis of all structural components of a large space platform is a prerequisite to control system design with particular regard to docking and reboost operations.

SASP Structure

When retracted, the SASP truss assumes an accordion-like configuration with the longitudinal, diagonal, and transverse members aligned as depicted in Fig. 2a. Deployment of the truss is made possible by the telescoping design of the main diagonals and the freedom of rotation of certain structural members at the joints. In the retracted position, the length of each telescoping diagonal is approximately 2.6 m. A deployment cable passes sequentially through each diagonal and across pulleys at the folding joints, and is attached to the end of the final truss bay. In deployment, the cable is reeled at constant speed by a motor located at the initial bay. This action produces shortening and rotation of the telescoping diagonals as in Fig. 2b. Simultaneously, the longerons rotate about pin connections at each joint, and the transverse members execute pure translation in following the joint motion. When a bay of the truss reaches the fully deployed position, a locking mechanism on the diagonals is actuated, thus locking each bay into its three-dimensional truss configuration.

Excepting the longerons, which have open cross sections designed for nesting, the structural members are made of aluminum tubing with 50.8 mm o.d. and 1.8 mm wall thickness. Physical properties of the various truss members are shown in Table 1. Joint fittings, payload carrier frames, and cable trays are of the same aluminum alloy. Each two-bay cell is composed of 26 members. Without payload carriers and

Table 1 Physical properties of structural members

	I_y, mm^4, $\times 10^5$	I_z, mm^4, $\times 10^5$	Mass, kg $\times 10^{-2}$	Length, m
External longeron	1.30	1.21	5.05	1.4
Internal longeron	1.46	2.80	5.29	1.4
Tube	0.84	0.84	3.40	1.4
Diagonal tube	0.84	0.84	4.86	1.98
Telescoping diagonal	0.84	0.84	9.00	1.98
		$E = 6.9 \times 10^4$ MPa		

accounting for end closure, the ten-bay, five-cell truss contains 135 structural members. Because of the deployment design, 102 members are pin-jointed.

SASP Finite Element Model

The specific objective of the work described herein was to ascertain the effects of the complex joint design on the modal characteristics of the truss. To accomplish this objective, a finite element model (SFEM) of the truss has been formulated which specifically incorporates the anomalies of joint geometry. Simultaneously, a "standard" finite element model using the Structural Performance Analysis and Redesign (SPAR) system[3] was developed for purposes of comparison. Both SFEM and SPAR formulations model the structural members as two-node, three-dimensional beam elements using the element stiffness matrix $\boldsymbol{k}_e$ and element consistent mass matrix $\boldsymbol{m}_e$ as given by Craig.[4] Each node has six degrees of freedom corresponding to three translations and three rotations about the translational axes. The 12 degrees of freedom for each element are represented by the element displacement vector $\boldsymbol{u}$.

To assemble the system stiffness and mass matrices, a global coordinate system having axes parallel to the major axes of the truss is used as shown in Fig. 1. The element displacement vector is transformed to the global system using

$$\boldsymbol{u} = \boldsymbol{A}\boldsymbol{u}_g \tag{1}$$

where $\boldsymbol{u}_g$ is the vector of element global displacements and $\boldsymbol{A}$ is the 12×12 transformation matrix composed of the direction cosines between element coordinates and global coordinates. Writing the element potential and kinetic energies

$$V = \tfrac{1}{2}\boldsymbol{u}^T\boldsymbol{k}_e\boldsymbol{u} \tag{2}$$

$$T = \tfrac{1}{2}\dot{\boldsymbol{u}}^T\boldsymbol{m}_e\dot{\boldsymbol{u}} \tag{3}$$

and utilizing Eq. (1) gives the element stiffness and mass matrices in the global system as

$$\boldsymbol{k} = \boldsymbol{A}^T\boldsymbol{k}_e\boldsymbol{A} \tag{4}$$

and

$$\boldsymbol{m} = \boldsymbol{A}^T\boldsymbol{m}_e\boldsymbol{A} \tag{5}$$

respectively.

The vector of system displacements $\boldsymbol{U}$ is composed of all pertinent translational and rotational displacements at each joint of the structure. The individual element displacements are related to system displacements by defining, for each element, a locator matrix $\boldsymbol{L}_e$ such that

$$\boldsymbol{u}_g = \boldsymbol{L}_e\boldsymbol{U} \tag{6}$$

Equation (6) does nothing more than assign each of the 12 element displacements to a particular system displacement, and $\boldsymbol{L}_e$ is composed strictly of zeros and ones in 12 rows and N columns, where N is the total number of system displacements (i.e., degrees of freedom).

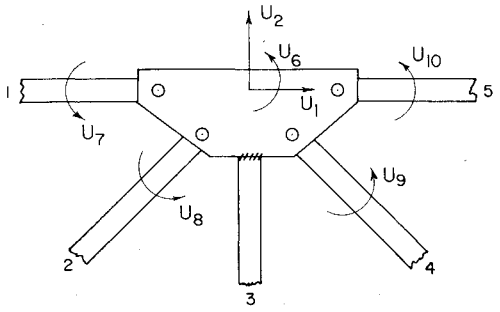

Fig. 3 Global displacements at truss joint in *XZ* plane.

The distinguishing characteristic of SFEM lies in the formulation of the system displacement vector. Normally $\boldsymbol{U}$ is composed of the six coordinate displacements (three translations, three rotations) at each joint in the structure. For the SASP truss this is not the case, because additional degrees of freedom exist at each joint because of the pin connections. To include these in the model, the method proposed by Winfrey[5] for analysis of elastic deformations in mechanisms is used. To illustrate, a plane view of one of the major joints of the SASP truss is shown in Fig. 3. In the plane depicted, the joint displacements are U_1, U_2, and U_6 corresponding to translation parallel to global axes Z and X, and rotation about global axis Y, respectively. However, of the structural elements shown in this view, only element 3 is attached such that its displacements correspond to those of the joint. Elements 1, 2, 4, and 5 have rotational freedom about the pin connections at the joint while their translational displacements are the same as the joint. In order to model the joint geometry of the SASP truss more accurately, four additional degrees of freedom are assigned corresponding to U_7 through U_{10} as shown. Using this procedure at each joint of the three-dimensional structure, it is found that a SASP truss composed of M bays has $24(M+1)$ system coordinates associated with standard joint displacements and $20M+4$ system coordinates corresponding to the additional rotational degrees of freedom.

As is shown by Fig. 3, the structural elements are pinned to a gusset plate and the pin joints are eccentrically located relative to the point of intersection of the element axes. This design is a necessary prerequisite for the deployment/retraction characteristics of the truss. As the eccentricity is small (75 mm) in comparison to element length, it has been neglected in the finite element models. Rather, the joints are modeled as if located at the intersection point. Thus, for the elements shown in Fig. 3, the SFEM joint has elements 1, 2, 4, and 5 attached to a pin fixed on element 3. In the SPAR model, the five elements are fixed to each other at the intersection point.

With the system coordinates defined and having assigned the various element displacements accordingly, assembly of the system equations of motion can be completed. The system potential energy is

$$V = \frac{1}{2}\sum_{e=1}^{N} \boldsymbol{u}_g^T \boldsymbol{k} \boldsymbol{u}_g \tag{7}$$

where N is the total number of elements in the structure. Using Eq. (6) for each element gives

$$V = \frac{1}{2}\sum_{e=1}^{N} \boldsymbol{U}^T \boldsymbol{L}_e^T \boldsymbol{k} \boldsymbol{L}_e \boldsymbol{U} \tag{8}$$

or

$$V = \frac{1}{2}\boldsymbol{U}^T\left(\sum_{e=1}^{N} \boldsymbol{L}_e^T \boldsymbol{k} \boldsymbol{L}_e\right)\boldsymbol{U} \tag{9}$$

as the potential energy expressed in system coordinates. The summation term in Eq. (9) is the assembled system stiffness matrix $\boldsymbol{K}$ such that

$$V = \tfrac{1}{2}\boldsymbol{U}^T\boldsymbol{K}\boldsymbol{U} \tag{10}$$

Similarly, the system consistent mass matrix is

$$M = \sum_{e=1}^{N} \boldsymbol{L}_e^T \boldsymbol{m} \boldsymbol{L}_e \tag{11}$$

and the system kinetic energy is then

$$T = \tfrac{1}{2}\dot{\boldsymbol{U}}^T\boldsymbol{M}\dot{\boldsymbol{U}} \tag{12}$$

Using Eqs. (10) and (12) to form the Lagrangian results in the system equations of motion in the expected form

$$\boldsymbol{M}\ddot{\boldsymbol{U}} + \boldsymbol{K}\boldsymbol{U} = 0 \tag{13}$$

Solution of the eigenvalue problem represented by Eq. (13) yields the natural frequencies and mode shapes for free vibrations of the truss.

Discussion

For ease of software development and debugging, the SASP finite element model was first applied to a single-cell, two-bay truss composed of 31 elements and constrained as a cantilever. The resulting structural model has 92 active degrees of freedom after elimination of 24 joint displacements via the constraint conditions. Computer programs were written to calculate the element stiffness and mass matrices sequentially, transform the matrices to the global coordinate system, and assemble the system stiffness matrices. The matrix multiplications involving $\boldsymbol{L}_e$ and its transpose do nothing more than locate terms from the element matrices into the proper row-column position of the system matrices. To accomplish this while avoiding numerous matrix multiplications involving mostly zeroes, a locator vector was used for each element. The locator vector contains simply the row-column data for element-to-system correspondence.

After assembly of the system matrices, the eigenvalue problem was solved via the diagonalization method of Jacobi. The actual software used is embodied in NASA's FORMA[6] matrix subroutine package. For the two-bay truss, SFEM produced the fundamental frequency as 27.9 Hz. For comparison, a SPAR model of the two-bay configuration, using identical elements but only the 48 standard joint degrees of freedom, gave a fundamental frequency of 50.6 Hz. These results indicate that the joint geometry of the SASP truss affects the dynamic characteristics significantly. Before proceeding with further analyses, SFEM was reduced to the SPAR model by eliminating the extra degrees of freedom as a check on the software. The resulting system natural frequencies were substantially identical to those given by SPAR and, on this basis, the accuracy of SFEM was established.

Extending SFEM to the full-size, ten-bay truss entailed a significant change in the computational approach. The ten-bay truss is composed of 135 structural members having 444 active degrees of freedom. As with most finite element formulations, the system matrices are sparsely populated, and routine algebraic manipulation (as in the Jacobi method) is prohibitive both in computation time and storage requirements. For computational efficiency, the software for the model was revised such that all matrix operations could be performed using partition logic. The conversion was readily accomplished because of the existence of a second NASA subroutine package (ZFORMA) containing partition logic matrix manipulation software. The eigenvalue problem for the ten-bay truss was then solved using a Rayleigh-Ritz iteration technique[7,8] with random generation of the initial eigenvector approximations.

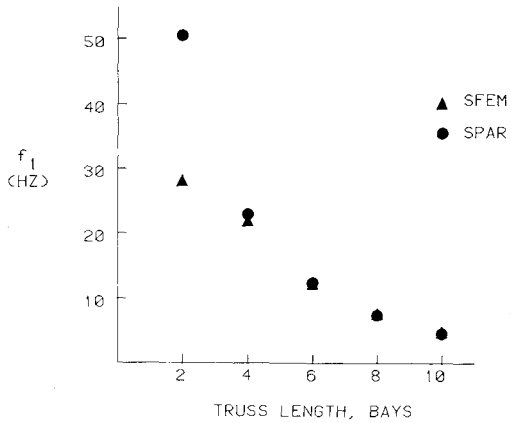

Fig. 4 Comparison of fundamental frequency as a function of truss length for the two finite element models used in the analysis.

Table 2 Modal frequency comparison for two-bay models

	Frequency, Hz	
Mode	SFEM	SPAR
1	27.85	50.42
2	28.03	58.35
3	28.13	63.31
4	28.14	70.96
5	37.16	76.32
6	38.20	79.71
7	38.31	80.22
8	50.56	85.11

Even in partition logic, the computational routine required about 15 min of CPU time to calculate the two lowest natural frequencies of the ten-bay truss. This was deemed acceptable, however, since the primary objective was to obtain the fundamental frequency which was found to be 4.6 Hz. Again for comparison, analysis of a ten-bay truss model using the SPAR system was undertaken. The SPAR model also gave the fundamental frequency as 4.6 Hz. The second frequency, 5.4 Hz, was also in agreement. Prior to accepting the results of the SFEM partition logic software, a check was obtained by reducing the model to the two-bay truss for comparison with the earlier results obtained by the Jacobi method. The check procedure produced the same 92 natural frequencies previously obtained for the two-bay truss. Thus the results of the two- and ten-bay truss models indicated a decreasing significance of pin joint degrees of freedom with increasing truss length.[9] This was verified by obtaining additional results from each model for four-, six-, and eight-bay truss lengths. A dual plot of fundamental frequency as a function of truss length (Fig. 4) clearly shows convergence of the results with increasing length.

The explanation for the convergence shown in Fig. 4 is found by analysis of differences in mode shapes exhibited by the two models as well as frequencies of the first few modes. Table 2 lists the natural frequencies of the first eight modes for a two-bay model with (SFEM) and without (SPAR) the extra degrees of freedom at pin joints. As shown, the first four modal frequencies from SFEM are clustered near 28 Hz. The corresponding mode shapes show that these modes are characterized primarily by vibration of the four telescoping diagonal elements. If mounted as simply supported beams, the fundamental frequency for these elements is about 25.4 Hz. The increase above this value and the slight differences in the four frequencies are attributable to the elastic properties of the pin connections. As would be expected, these four modes do not contribute appreciably to overall truss motion. Similarly, modes 5 through 7 have frequencies near 38 Hz. These modes are characterized by beam-type vibration of the three transverse diagonal elements parallel to the global *XY* plane of Fig. 1. The corresponding simple-beam frequency is 34.5 Hz. These modes also have no significant affect on overall motion.

Table 3 Modal frequency comparison for four-bay models

SFEM		SPAR	
Mode	Frequency, Hz	Mode	Frequency, Hz
1	21.57	1	22.62
2	24.53	2	26.28
3–10	27.4–31.5		
11–15	37.9–40.3		
16	43.08	3	42.28

Mode 8 is the first SFEM-generated mode which exhibits general truss motion. The mode shape is basically that of a cantilever beam oscillating in the *YZ* plane and exhibiting slight torsional motion due to the lack of axial symmetry. The modal frequency of 50.56 Hz is very near the SPAR model mode 1 frequency of 50.42 Hz. Comparison of the mode shapes generated by the two models at these frequencies shows that the truss motions represented are almost identical. Similar comparison of additional higher-order mode shapes for which the two models produce near-equal frequencies also shows nearly identical motions with only minor differences attributable to the pin-jointed members.

Table 3 shows modal frequency data for SFEM and SASP models of the four-bay truss. For purposes of comparison, the SFEM frequencies which are primarily attributable to oscillations of pin-jointed elements have been grouped together. Modes 3 through 10, with frequencies banded around 29 Hz, are those for which the major motion components are the eight telescoping diagonal elements of the four-bay truss. Similarly, modes 11 through 15 are indicative of motion associated primarily with the five transverse diagonal elements. The data also shows that SFEM modal frequencies 1, 2, and 16 are in relatively close agreement with those of SPAR modes 1, 2, and 3. Analysis of the mode shapes shows that each of these sets of three frequencies represent the same three modes of truss motion. It is also noted that these modes correspond to global motion of the truss as opposed to individual elements. Thus the results show that the length of the four-bay truss is such that the lowest frequency of global truss motion is lower than that of motion associated primarily with pin-jointed elements. That this is not the case for the shorter two-bay truss substantiates the convergence phenomenon of Fig. 4.

Conclusions

A detailed finite element analysis of the SASP deployable truss has shown that the fundamental frequency of vibration of the cantilever truss configuration is not affected significantly by the additional degrees of freedom associated with the many pin-jointed structural elements, except for relatively short overall truss lengths. The results of the analysis lead to the conclusion that simplified models based on the SPAR system can be used to adequately assess the dynamic characteristics of the structure for those configurations being considered for the Structural Assembly Demonstration Experiment.

As additional deployable truss designs evolve or composite platform configurations using the SASP truss are considered, similar analyses should be conducted to ensure the accuracy of simplified models. Detailed modeling similar to SFEM might be required if, for example, a platform concept includes short truss sections for payload attachment.

Acknowledgments

The work described in this paper was supported by the NASA/ASEE Summer Faculty Fellowship Program at the NASA Marshall Space Flight Center, Huntsville, Ala. The author also wishes to express his appreciation to MSFC's Dr. John R. Admire for his considerable assistance with software problems during the course of the investigation.

References

[1]Haggerty, J.J., "'SPACE STATION' The Next Logical Step," *Aerospace*, Vol. 20, No. 3, 1982, pp. 2–9.

[2]Stoll, H.W., "Computer Simulation for Dynamic Analysis of a Deployable Space Structure," Final Report, NASA Contract NAS8-34506, Sept. 1981.

[3]"SPAR Structural Analysis System Reference Manual," NASA CR158970-2, 1978.

[4]Craig, R.R. Jr., *Structural Dynamics*, John Wiley & Sons, New York, 1981, Chap. 16.

[5]Winfrey, R.C., "The Finite Element Method as Applied to Mechanisms," *Finite Element Applications in Vibration Problems*, ASME, New York, 1977, pp. 19–39.

[6]Wohlen, R.L., "Expansion and Improvement of the FORMA System for Response and Load Analysis," NASA MCR-76-217, May 1976.

[7]Clough, R.W. and Penzien, J., *Dynamics of Structures*, McGraw-Hill Book Co., New York, 1975, Chap. 14.

[8]Admire, J.R., "Modal Analysis of Structures by an Iterative Rayleigh-Ritz Technique," NASA TM X-64528, 1970.

[9]Hutton, D.V., "Finite Element Analysis of a Deployable Space Structure," NASA CR-162051, Aug. 1982.

From the AIAA Progress in Astronautics and Aeronautics Series...

ENTRY HEATING AND THERMAL PROTECTION—v. 69

HEAT TRANSFER, THERMAL CONTROL, AND HEAT PIPES—v. 70

Edited by Walter B. Olstad, NASA Headquarters

The era of space exploration and utilization that we are witnessing today could not have become reality without a host of evolutionary and even revolutionary advances in many technical areas. Thermophysics is certainly no exception. In fact, the interdisciplinary field of thermophysics plays a significant role in the life cycle of all space missions from launch, through operation in the space environment, to entry into the atmosphere of Earth or one of Earth's planetary neighbors. Thermal control has been and remains a prime design concern for all spacecraft. Although many noteworthy advances in thermal control technology can be cited, such as advanced thermal coatings, louvered space radiators, low-temperature phase-change material packages, heat pipes and thermal diodes, and computational thermal analysis techniques, new and more challenging problems continue to arise. The prospects are for increased, not diminished, demands on the skill and ingenuity of the thermal control engineer and for continued advancement in those fundamental discipline areas upon which he relies. It is hoped that these volumes will be useful references for those working in these fields who may wish to bring themselves up-to-date in the applications to spacecraft and a guide and inspiration to those who, in the future, will be faced with new and, as yet, unknown design challenges.

Volume 69—361 pp., 6×9, illus., $22.00 Mem., $37.50 List
Volume 70—393 pp., 6×9, illus., $22.00 Mem., $37.50 List

TO ORDER WRITE: Publications Dept., AIAA, 1633 Broadway, New York, N.Y. 10019